Macromolecules

Article

pubs.acs.org/Macromolecules

Chain Exchange Kinetics of Asymmetric B_1AB_2 Linear Triblock and AB_1B_2 Branched Triblock Copolymers

Andrew J. Peters[†] and Timothy P. Lodge*[,†,‡]

[†]Department of Chemistry and [‡]Department of Chemical Engineering and Materials Science, University of Minnesota, Minneapolis, Minnesota 55455, United States

Supporting Information

ABSTRACT: Equilibrium chain exchange of asymmetric B_1AB_2 and AB_1B_2 branched triblock copolymers in a B selective solvent has been studied via dissipative particle dynamics simulations. Hybridization simulations are performed using B_1AB_2 and AB_1B_2 branched triblock copolymers at varying levels of asymmetry and compared with equivalent AB diblock copolymers. It is found that B_1AB_2 triblocks exchange ∼1 order of magnitude faster than diblocks (persisting over various values of χN_{core} and total corona length), while AB_1B_2 triblocks exchange ∼4 times faster than diblocks. The dependence on asymmetry is weak, with very asymmetric triblocks ($N_{B_1} \ll N_{B_2}$) exchanging only 2 or 3 times faster than symmetric triblocks. Two causes are found for this: (1) increases in the density of corona beads near the micelle core for triblocks, resulting in greater stretching penalties and lower aggregation numbers, and (2) looped core blocks (B_1AB_2) spending more time near the surface of a micelle core than unlooped core blocks (AB_1B_2 and AB), resulting in a lower energy benefit of insertion. Additionally, unlooped core blocks pull out bead-by-bead with multiple activations, whereas the looped core blocks tend to aggregate near the micelle surface and pull out as a single entity, potentially further reducing the energy penalty of pullout. Because of this difference in mechanism, the looped core triblocks pull out more rapidly than the unlooped core triblocks even at identical aggregation numbers.

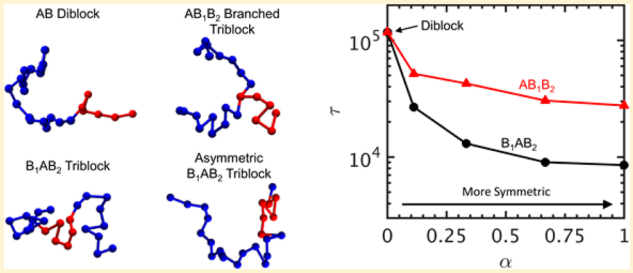

INTRODUCTION

Block polymers exhibit a wide array of interesting properties due to their ability to undergo microphase separation at various length scales. When the simplest example, a linear diblock copolymer composed of only two distinct chemical regions, is dissolved in a selective solvent, these polymers can form micelles.[1−3] Such structures are used in a variety of applications, including controlled drug delivery,[1,3,4] viscosity modification,[5,6] and polymer blend stabilization.[7] Critical to controlling polymer self-assembly and behavior is a thorough understanding of the chain exchange processes that are essential to achieving equilibrium. As such, significant experimental and computational effort has been directed at understanding this process. Experimental techniques as varied as time-resolved light scattering,[8] small-angle neutron scattering (SANS),[9−13] small-angle X-ray scattering,[14] stopped-flow light scattering,[15−17] fluorescence-quenching techniques,[17,18] and small-amplitude oscillatory rheometry[1,9,20] have been used to study these rates of chain exchange, while computational techniques such as dissipative particle dynamics (DPD),[21−25] Monte Carlo,[26] and self-consistent field theory (SCFT)[27] have also been used.

In the case of diblocks, micelle chain exchange has been studied as a function of polymer length, interactions between polymer blocks and/or solvents, concentration, and dispersity. It has been found that the exchange rate exhibits a hypersensitivity to core chain length,[9] wherein a 38% decrease in block length led to a 3−4 order of magnitude decrease in relaxation time, which was the result of an "exponential of an exponential" dependence of the relaxation function on core block length.[9,12] When dispersity is involved, the distribution of relaxation times caused by the variations in core block length results in a decay that is approximately logarithmic in form.[9,28] The effect of the corona block length has been less clear, with reports of both an increase[29] and a decrease in chain exchange rate as corona block length increases.[30] The strength of interactions between the core block and the solvent, as described by the Flory−Huggins χ parameter, has been shown to exhibit the same hypersensitivity as core block length; that is, chain exchange is strongly dependent on the product χN_{core}.[31] Since χ can be varied by changing temperature as well as solvent composition, varying either parameter can result in changes in the chain exchange rate of many orders of magnitude.[9,31−33]

While diblock chain exchange has been extensively studied, exchange of triblocks or more complicated polymer architectures has received less attention. Recently, Lu et al.[11] used TR-SANS to study chain exchange of symmetric A_1BA_2 and B_1AB_2

Received: May 18, 2017
Revised: July 24, 2017
Published: August 11, 2017

DOI: 10.1021/acs.macromol.7b01046
Macromolecules 2017, 50, 6303−6313

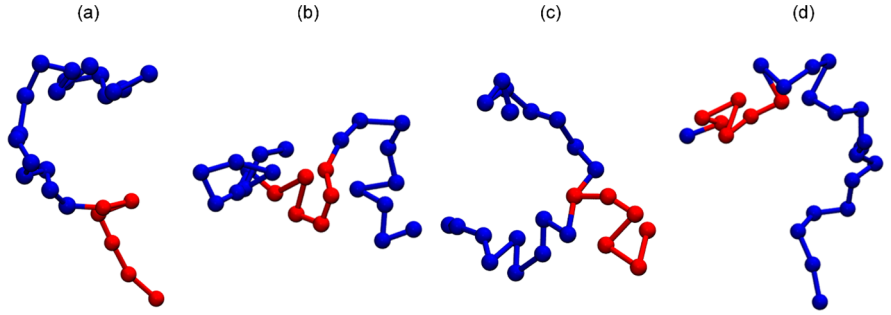

Figure 1. Snapshot of four types of polymers studied here: (a) linear AB diblock, (b) symmetric B_1AB_2 triblock polymer, (c) AB_1B_2 triblock polymer, and (d) asymmetric B_1AB_2 triblock polymer. Asymmetric AB_1B_2 polymers were also studied. The A-type beads (core-forming) are shown in red, and B-type beads (corona-forming) are shown in blue.

architectures in dilute solution (symmetric means $N_{A_1} = N_{A_2}$ and $N_{B_1} = N_{B_2}$). The A_1BA_2 polymers form flower-like micelles[19,34,35] where both end blocks insert into the same core and the midblock loops in the corona. This results in significantly slower exchange compared to a diblock that is half the length of the triblocks. In contrast, for B_1AB_2 polymers the A blocks loop in the core, which results in significantly faster chain exchange than diblocks with a core block of equal length to that of the triblock and a corona block of equal length to one of the triblock corona blocks. Prhashanna and Chen[25] reproduced this rapid B_1AB_2 exchange using DPD and found that most B_1AB_2 core blocks loop back on themselves in a micelle (as opposed to stretching across the micelle core), but the cause of the rapid B_1AB_2 exchange is still unclear. Is it due to the looped core block or to the fact that the corona block is now tethered to the core block surface in two locations?

In order to elucidate the effects of these two differences, two variations on the linear B_1AB_2 triblock copolymer used by Lu et al.[11] are considered, in addition to an AB diblock (Figure 1a) and a symmetric B_1AB_2 triblock (Figure 1b): (i) an AB_1B_2 branched triblock polymer (Figure 1c), in which both corona blocks are attached to the same end of the core block, instead of opposite ends as in the linear B_1AB_2 triblock, and (ii) asymmetric corona blocks of both B_1AB_2 and AB_1B_2 triblock polymers, that is, triblock polymers with two corona blocks of different length (Figure 1d). DPD simulations of both B_1AB_2 and AB_1B_2 polymers should help elucidate the effect of core-block looping, while variations in asymmetry will redistribute the corona blocks around the micelle core and help reveal corona stretching effects.

SIMULATION METHODOLOGY AND DETAILS

To model triblock polymer exchange, dissipative particle dynamics (DPD) simulations were used.[36,37] These simulations are well suited to study the kinetics and thermodynamics of block polymer assembly and have been used extensively in the literature.[21,22,38−41] We model three types of polymers: AB diblocks, B_1AB_2 triblocks, and AB_1B_2 branched triblocks. The A blocks form the micelle cores, and the B blocks form the micelle coronas. The AB_1B_2 polymers have the same overall composition as the B_1AB_2 polymers, but the bonds connecting the B blocks to the A block occur at the same end of the linear A block, as opposed to opposite ends as in the B_1AB_2 case, as shown in Figure 1. Each polymer was modeled as a chain of beads (coarse-grained units), where each bead represents a group of several atoms, and is typically much larger than a polymer repeat unit.[42] B_1AB_2 polymers are denoted as B_1AB_2 $N_{B_1}-N_{core}-N_{B_2}$ where N_i is the number of beads in a block. B_1 refers to the shorter of the two end blocks. $N_{B,total}$ refers to the total number of B beads in a polymer. AB_1B_2 polymers are denoted in the same way. When changing the relative lengths of the corona blocks on a triblock polymer, that is, when changing the asymmetry, a set of polymers with identical total numbers of A beads and B beads are referred to as a series. Series are denoted as B_1AB_2 A_i-B_i, where A_i refers to the number of A beads and B_i refers to the total number of B beads. Thus, the B_1AB_2 6−18 series consists of a number of polymers all with an A block of 6 A beads and a total of 18 B beads distributed between the two corona blocks. AB_1B_2 series are referred to analogously. The equivalent diblock (that is, the diblock with the same number of total A and B beads) is also included in each series for comparison. In this work, all polymers contain 6 A beads.

Bonds between beads were modeled using harmonic springs, $F_{ij}^S = (1/2)K(r_{ij} - r_0)^2$, where $K = 100$, r_{ij} is the separation distance between two beads, and $r_0 = 1$ is the equilibrium bond length. All beads have an identical mass 1. The pairwise forces between beads in DPD simulations were determined by

$$F_i = \sum_{i \neq j} F_{ij}^C + F_{ij}^D + F_{ij}^R \tag{1}$$

where F_{ij}^C are the conservative forces, F_{ij}^D is the dissipative force, and F_{ij}^R is a random force.[37,43] This force is only applied when two beads are within the cutoff distance, $r_c = 1$. The definitions of F_{ij}^C, F_{ij}^D, and F_{ij}^R are given in ref 37 and implemented using HOOMD's[44−46] pair.dpd potential with an F_{ij}^D coefficient (γ) of 3.[21,37] A repulsive conservative interaction is used and defined as

$$F_{ij}^C = \begin{cases} a_{ij}(1 - r_{ij})\hat{r}_{ij} & r_{ij} \text{ [[mml:lt]] } r_c \\ 0 & r_{ij} \geq r_c \end{cases} \tag{2}$$

The conservative interaction force coefficients a_{ij} for like beads was set at 25, which effectively reproduces the compressibility of water at room temperature, as done previously.[21,22,24,37] The B bead−solvent coefficient (a_{BS}) was set to 25 as well. The other unlike bead coefficients (a_{AB}, a_{AS}) were varied between 36.67 and 41 in order to vary the Flory−Huggins interaction parameter. These coefficients can be related to χ via[37]

$$\chi_{ij} = 0.286\Delta a_{ij} = 0.286(a_{ij} - a_{ii})$$

This set of parameters means that the micelles will form with A core blocks and B corona blocks, since the A blocks are more

DOI: 10.1021/acs.macromol.7b01046
Macromolecules 2017, 50, 6303−6313

strongly repulsed by the solvent. Mass, distance, energy, and time are scaled by m, r_c, k_BT, and $\sqrt{mr_c^2/k_BT}$, respectively.

All simulations were run at a polymer volume fraction of 0.05. The solvent was explicitly modeled using the same B beads that make up the polymers. Simulation box sizes were 30 × 30 × 30, except in the case of mixed triblock and diblock systems, where the simulations were 82 × 82 × 82 to allow for better statistics at low concentrations of the minority polymer. The NVT ensemble with $k_BT = 1$ and a time step of 0.04 was used. Simulations were initialized by randomly placing the solvent beads and polymers in the simulation volume with a minimum separation distance of 0.1 and a bond length of 1. Simulations were then run for 1.6×10^6 time units in order to achieve adequate sampling after reaching equilibration. Aggregates were identified using a distance criterion,[21,47] where any pairs of A beads within a cutoff distance of 1.5, and all beads that are part of the same chains as those beads, were designated to be in the same aggregate. Equilibrium is determined as stability in the average aggregation number.

RESULTS AND DISCUSSION

Chain Exchange Rates of B_1AB_2 and AB_1B_2 Polymers. After equilibration, chain exchange is quantified using the hybridization technique described in ref 22. At time $t = 0$ (an arbitrary time after equilibrium is reached) all chains in a given micelle are labeled as blue or red, such that approximately half of all micelles (including unimers and dimers, and therefore all chains) are labeled as blue or red. As chains exchange, these initially completely red or blue micelles become more and more a mix of blue and red chains, analogous to the mixing of deuterated and nondeuterated chains in the time-resolved SANS technique used experimentally.[9−12] This exchange is described using an autocorrelation function $I(t)$:

$$I(t) = 4\left\langle \sum\left[\left(\frac{N_r(t)}{N(t)} - \frac{1}{2}\right)^2 \frac{N(t)}{N_{total}}\right]\right\rangle \quad (3)$$

which is analogous to the scattering intensity change over time found experimentally.[9,11,12] $N_r(t)$ is the number of red chains in a micelle at time t, $N(t)$ is the total number of chains in a micelle at time t, and N_{total} is the total number of chains in the simulation. The ⟨...⟩ denotes ensemble averaging over different initial states. At time $t = 0$, all micelles are completely red or blue, and so $I(t) = 1$. As time progresses, I decays toward zero. Because of slight mismatches in the number of blue and red chains, statistical effects of chain distribution between micelles, and limited simulation size, $I(t)$ never reaches zero.

To eliminate this effect, a contrast function $C(t)$ is defined as done previously:[22]

$$C(t) = \left[\frac{I(t) - I(\infty)}{I(0) - I(\infty)}\right]^{1/2} \quad (4)$$

This is analogous to the relaxation function used to analyze chain exchange in TR-SANS experiments of diblock and triblock copolymers.[9,11,12] $I(\infty)$ is calculated by randomly setting each chain to be blue or red at each time step after equilibration, calculating an $I_\infty(t)$ for that time step, and then averaging over all I_∞ values. A representative plot of $C(t)$ is shown in Figure 2 for the B_1AB_2 6−18 series using an a_{AB} of 39, resulting in a χN_{core} of 24. The thermodynamic segregation χN_{core} has been shown to largely determine the time scale of exchange for diblock copolymers.[9,22] Time scales of relaxation are extracted using single exponentials (dashed lines), which fit the data well indicating a single time scale of relaxation dominates as previously found for monodisperse diblocks.[12,22,24]

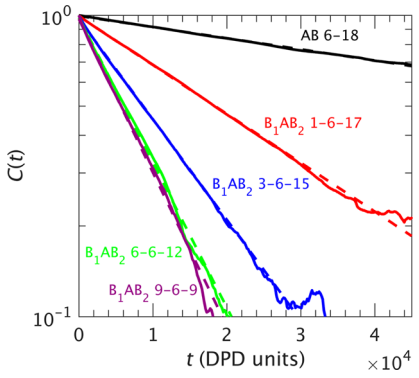

Figure 2. $C(t)$ for the B_1AB_2 6−18 series, with $\chi N_{core} = 24$. Dashed lines show single-exponential fits.

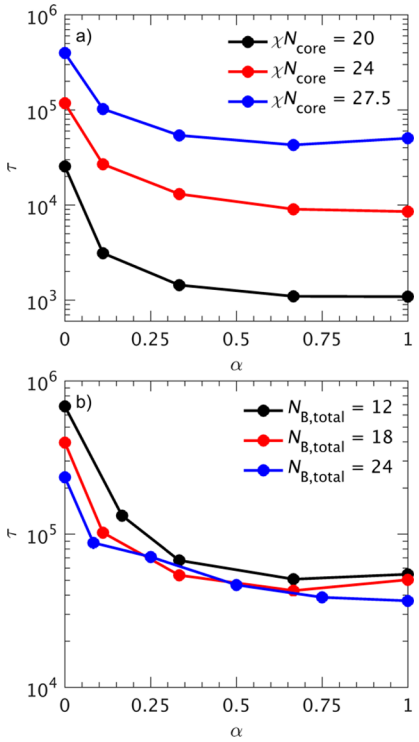

Figure 3. Relaxation time τ for B_1AB_2 triblocks as a function of α for (a) various χN_{core} with $N_{B,total} = 18$ and for (b) various total corona bead numbers ($N_{B,total}$) at $\chi N_{core} = 27.5$.

The extracted time scales (τ) are plotted in Figures 3 and 4 as a function of an asymmetry parameter α:

$$\alpha = 2\frac{N_{B_1}}{N_{B,total}} \quad (5)$$

where N_{B_1} is the length of the shorter B block and $N_{B,total}$ is the total number of B beads in the polymer. In the case of a diblock, $N_{B_1} = 0$ and so $\alpha = 0$. For a symmetric B_1AB_2 triblock such as B_1AB_2 9−6−9, $\alpha = 1$. Any $\alpha > 0$ indicates a triblock,

DOI: 10.1021/acs.macromol.7b01046
Macromolecules 2017, 50, 6303−6313

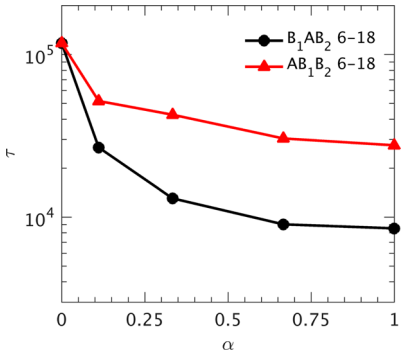

Figure 4. Comparison of τ for B_1AB_2 6−18 and AB_1B_2 6−18, with χN_{core} = 24. Both show a similar shape, but the AB_1B_2 triblock is significantly slower in all cases.

where smaller α values indicate a more asymmetric polymer and larger values indicate a more symmetric polymer. An increase in α can be imagined as the transfer of beads from the larger B block to the smaller B block or, in the case of a diblock, a transfer of beads from the B block to create a new block. Figure 3a shows τ for the B_1AB_2 6−18 series at a_{AB} values of 36.67, 39, and 41, resulting in χN_{core} values of 20, 24, and 27.5. Figure 3b shows extracted τ values for the series using 6 A beads and various total number of B beads at a χN_{core} of 27.5.

The large drop in τ from diblock (α = 0) to symmetric B_1AB_2 triblock (α = 1) is qualitatively consistent with experimental results, which showed a 3 orders of magnitude difference in chain exchange time between a poly(styrene-*b*-(ethylene-*alt*-propylene)) SEP diblock copolymer and a symmetric SEPS triblock copolymer.[11] Additionally, the strong overall dependence of τ on χN_{core} is consistent with previous simulations[24] and experiments,[9] which show dependences of $\tau \sim e^{0.67\chi N_{core}}$ and $\tau \sim e^{0.6\chi N_{core}}$, respectively, comparable though slightly greater than the scaling for symmetric triblocks found here: $\tau \sim e^{0.51\chi N_{core}}$. All three scalings result in an order of magnitude change in exchange time when χN_{core} is varied by a value of 3 to 5. Increasing the corona block length increases the rate of exchange, an effect most evident in diblocks (α = 0). Previous results on this point are apparently contradictory, with some simulations[22] and experiments[48] yielding an increase in rate with increased corona block length as seen here and other simulations[25] and experiments[30] yielding a decrease in rate. This discrepancy is likely caused by competition between two effects: an increased drive for expulsion for longer coronas caused by a more crowded and stretched corona, and a decreased diffusivity through the corona with longer corona blocks resulting in a greater chance of reinsertion.[25,30,49] In this case, the increase in exchange rate with increased corona block composition seen in diblocks persists in triblocks as well, though the effect is weaker. For example, the AB 6−24 diblock exchanges ∼2.9 times faster than the AB 6−12 diblock, but the B_1AB_2 12−6−12 symmetric triblock exchanges only ∼1.5 times faster than the B_1AB_2 6−6−6 symmetric triblock. Most interesting is the overall shape of each curve with increasing α. In all cases, a large drop in τ occurs as the first bead is moved to form a triblock, but subsequent additions make a relatively small difference. The first α value >0 for each series is for the triblock polymer where the shorter B block contains only one bead, and this single bead makes the largest change in the overall chain exchange time. After χN_{core}, the overall triblock architecture is the primary determiner of relaxation time, while the asymmetry makes little difference, and this behavior persists over a range of χN_{core} and $N_{B,total}$.

The same hybridization experiment and analysis was performed on the AB_1B_2 triblocks, and the resulting τ values for AB_1B_2 6−18 and B_1AB_2 6−18 with χN_{core} = 24 are shown in Figure 4. These polymers exhibit an altered distribution of corona blocks compared to B_1AB_2 polymers but also retain the unlooped core block of the diblock copolymers. In this way, the effects of corona block redistribution can be separated from core block looping. Both B_1AB_2 and AB_1B_2 polymers show the same qualitative shape, a sharp change at low α and little change at higher α, but the AB_1B_2 triblocks exchange significantly more slowly than the B_1AB_2 triblocks. This indicates that both differences, looping of the core block and altered corona block distributions, play important roles in chain exchange. If we compare the diblock τ to the symmetric triblock τ, the relative importance of each component can be considered: $\tau_{AB\,6-18}/\tau_{AB_1B_2\,6-9-9}$ = 4.25 while $\tau_{AB_1B_2\,6-9-9}/\tau_{B_1AB_2\,9-6-9}$ = 3.24, suggesting that the two effects are similar in magnitude for this system. The details of these characteristics and their effects on chain exchange will be considered in greater detail subsequently.

Effect on Thermodynamic Properties. It is unclear under what conditions chain exchange is determined by thermodynamic properties or by large kinetic barriers; some experiments report that exchange is significantly affected by altering corona chain stretching (and therefore entropy of the inserted state, a thermodynamic property),[50] while others report that exchange is significantly affected by the rate of diffusion through the micellar corona (a kinetic barrier).[51] Considering the effects of polymer architecture on aggregation number (N_{agg}) and the unimer fraction (f_{unimer}) will help answer the question of whether or not the changes in chain exchange rate caused by the triblock architecture are due to thermodynamic or kinetic factors. The number-averaged micelle aggregation number distribution for the B_1AB_2 6−18 series (χN_{core} = 24) is shown in Figure 5a. Each polymer shows a single peak with a large increase below $N_{agg} \sim 3$, indicating the presence of unimers, dimers, and small aggregates in significant concentration. As α increases, the distributions shift toward smaller N_{agg}. Interestingly, the distribution for triblocks appears to narrow at high α, perhaps because of a higher stretching penalty per chain (as discussed later, these chains have a higher corona block density (d), which would increase the stretching penalty per inserted chain). Similar trends are found for the N_{agg} distribution of AB_1B_2 polymers, which can be found in the Supporting Information. A Gaussian distribution is fit to each series (neglecting the upturn at low N_{agg}), and the resulting mean is plotted in Figure 5b. This average aggregation number $\bar{N}_{agg}$ follows a very similar trend as τ: a relatively sharp decrease at low α followed by relatively small decreases at higher α, and AB_1B_2 polymers have larger $\bar{N}_{agg}$ just as they had larger τ. Similarly, f_{unimer}, shown in Figure 6, increases as α increases but begins to level off at larger α. Again, AB_1B_2 polymers exhibit a smaller change from diblocks compared to B_1AB_2 polymers. The behaviors of both $\bar{N}_{agg}$ and f_{unimer} are consistent with the behavior of τ, as they both indicate a reduction in the free energy of the inserted state and an increase in the rate of chain exchange. It therefore appears that this exchange is primarily determined by thermodynamic properties, with smaller aggregation numbers, larger unimer concentrations (and therefore critical micelle concentration),

DOI: 10.1021/acs.macromol.7b01046
Macromolecules 2017, 50, 6303−6313

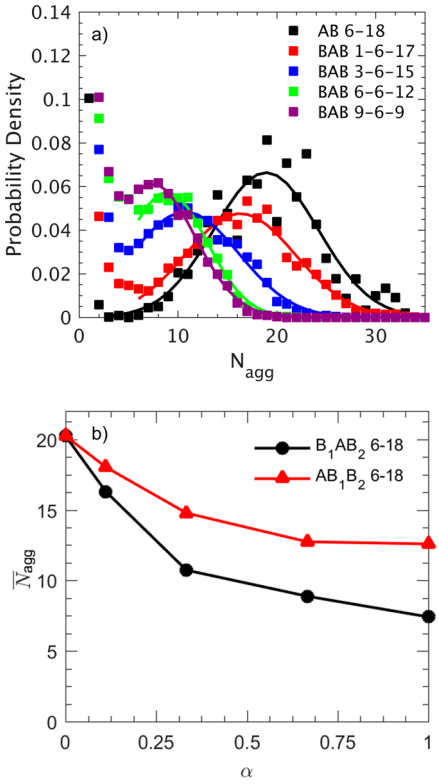

Figure 5. (a) Distribution of aggregation numbers for the B_1AB_2 6−18 series, with χN_{core} = 24. Gaussian fits (neglecting the upturn at low N_{agg}) are shown as solid lines. (b) Mean aggregation number ($\bar{N}_{agg}$) taken from Gaussian fits for both B_1AB_2 and AB_1B_2 distributions; AB_1B_2 distributions can be found in the Supporting Information.

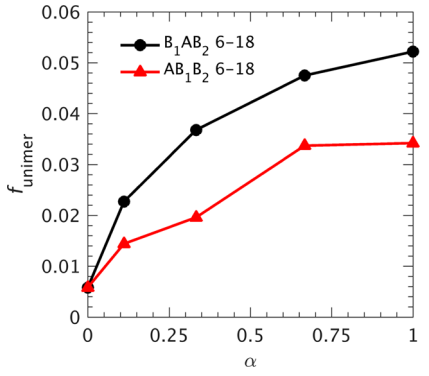

Figure 6. Unimer fraction (f_{unimer}) for B_1AB_2 6−18 and AB_1B_2 6−18 as a function of α; χN_{core} = 24.

and consequently faster chain exchange in both AB_1B_2 and B_1AB_2 triblocks compared to similar diblocks. We will now consider in detail how the altered corona distribution and core block looping affect these thermodynamic properties and the chain exchange rate.

Effect of Corona Bead Redistribution. As previously noted, there are at least two contributions to the faster chain exchange in the triblocks: corona stretching and core block looping. Since thermodynamic properties and chain exchange both change substantially when making a triblock at constant composition and total chain length, but less so as the corona block is redistributed within the triblock, it is likely that corona stretching and core block looping follow the same trend: large changes when first forming a triblock and smaller changes after redistributing B blocks among two existing blocks. First we will consider corona stretching. In the field of polymer brushes and polymer-grafted nanoparticles, the grafting density $\left(\sigma = \frac{\text{no. of chains}}{\text{surface area}}\right)$ is often used to describe the perturbation a chain undergoes in such an environment.[52−55] In the case of micelles, we can use an analogous parameter, corona block density d, which is equal to the number of corona blocks per micelle core surface area ($d = \frac{\text{no. of corona blocks}}{\text{surface area}}$, where the surface area is calculated assuming a spherical micelle), to describe the perturbation to the corona upon inserting a chain. The resulting d values for both the B_1AB_2 6−18 and AB_1B_2 6−18 (χN_{core} = 24) series are shown in Figure 7. This density

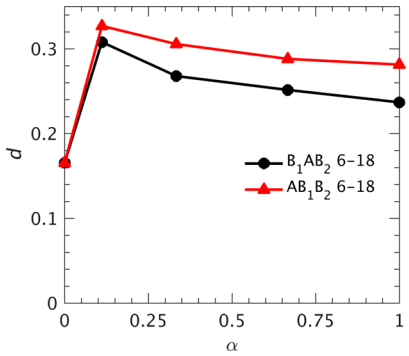

Figure 7. Corona block density (d) for B_1AB_2 and AB_1B_2 6−18; χN_{core} = 24.

increases sharply as the polymers are changed from diblock to triblocks because the number of corona blocks doubles for a given $\bar{N}_{agg}$. Even though $\bar{N}_{agg}$ decreases from diblock to triblock, the doubling of corona blocks overcomes this small decrease to result in an overall net increase in d. After this sharp increase, d slightly decreases with α because $\bar{N}_{agg}$ decreases, but d still remains above the diblock value. The sharp increase from diblock to triblock in Figure 7 is consistent with the sharp drop in τ and corresponding changes in $\bar{N}_{agg}$ and f_{unimer}. A more crowded corona, corresponding to a higher d, would result in a greater free energy penalty for the corona block in the inserted state, leading to smaller aggregates and more rapid chain exchange. The larger d values for AB_1B_2 compared to B_1AB_2 arise because the unlooped core block favors a larger $\bar{N}_{agg}$, as will be discussed later. There are two main limitations to this analysis: (i) a very short block ($B_1 \ll B_2$) is treated equivalently as a longer block ($B_1 \approx B_2$), and (ii) it does not distinguish between corona beads close to the core surface and those farther away. Because the density of the corona block is highest near the core, the beads restricted close to the core surface contribute more to the net crowding of the corona block, and sections near the core will be more stretched. To account for these limitations, and to consider the detailed ramifications of the corona block distribution, the radial density of the corona blocks was measured.

The radial density of beads relative to the core for B_1AB_2 6−18 at χN_{core} = 24 is plotted in Figure 8; the corresponding AB_1B_2 data are shown in Figure S2. AB_1B_2 polymers have slightly higher corona densities due to the higher $\bar{N}_{agg}$ values, but otherwise the results are similar. Figure 8a shows the density of all corona beads within one micelle, Figure 8b shows the density of the longer chains in the corona, and Figure 8c shows the density of the shorter chains. The diblock corona

DOI: 10.1021/acs.macromol.7b01046
Macromolecules 2017, 50, 6303−6313

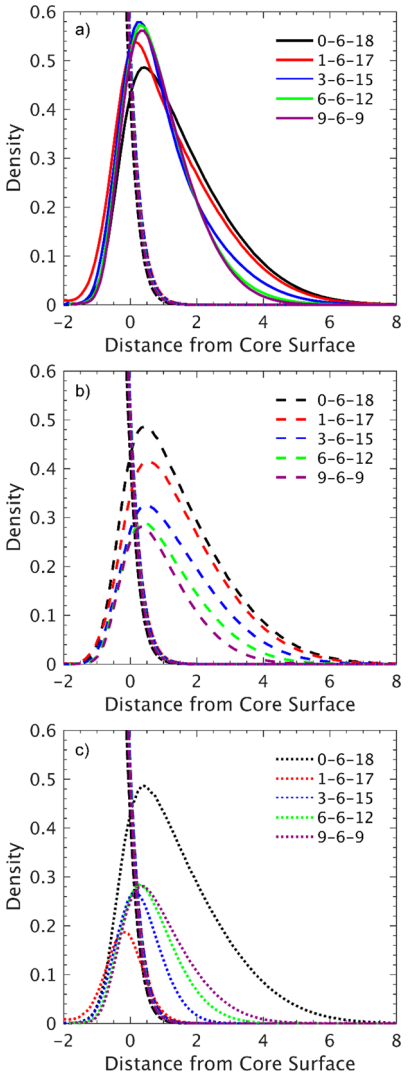

Figure 8. Radial density of beads relative to core for B_1AB_2 6−18; χN_{core} = 24. Equivalent data for AB_1B_2 6−18 are shown in the Supporting Information. The core surface is defined as the point at which the A and B bead densities are equal. The A bead density is shown as dash-dotted lines in each plot for reference. (a) shows the density of all B beads, (b) shows the density for long B blocks only, and (c) shows the density for short B blocks only. In (c), the single B block in the diblock density is shown for reference.

densities are always shown for all corona beads, for reference. The densities are taken relative to the surface of the micelle core, which is defined as the point where the densities of the A core beads and the B corona beads are equal. The core density is shown as dash-dotted lines for reference and reaches a maximum density of 3.26, just above the average overall density of 3. In Figure 8a, the peak locations of the triblocks are all slightly left of the diblock peak. This is reasonable, as to make the triblocks, the outermost beads in the B block are reattached to the A block and forced to the surface of the core, or even inside the core, which is enthalpically unfavorable. As α increases among the triblocks, the peaks shift back to the right, although always remaining to the left of the diblock peak. This is in part because the outmost beads are now being moved, not right onto the micelle core, but some distance away at the end of the shorter block. As the density in that region increases, the peak density can shift back out slightly. This can be seen by comparing Figures 8b and 8c. The peak location of the longer chains (Figure 8b) shifts left (toward the core) as the endmost beads are removed, while the peak locations of the shorter chains (Figure 8c) shift right (away from the core) as the beads are added to the end of the shorter block, allowing them to extend farther from the core. In addition, the larger drive to be excluded from the core (because χN for the short blocks increases as they lengthen) causes the left-hand side of the density distribution for the short chains to move away from the core as α increases. In the case of B_1AB_2 1−6−17, the short chain peak density is inside the micelle core, indicating that these beads spend most of their time just inside the core. This effect actually results in the left-hand side of the distribution for B_1AB_2 1−6−17 being slightly left of all the other distributions. The right-hand tail of the overall distribution (Figure 8a) also shifts left as the outermost beads are shifted closer to the core. Figure 8b shows the longer blocks decreasing in density (because of fewer beads and a smaller aggregation number) and losing the outermost extent as the shortened chains cannot extend as far.

The maximum corona density is higher for the triblocks than the diblocks, consistent with d shown in Figure 7. As with d, the maximum corona density increases significantly from diblock to triblock. However, unlike d, which decreases slightly as α increases, the maximum density continues to increase until N_{B_1} = 3 (α = 1/3). At higher α both d and corona density slightly decrease because $\bar{N}_{agg}$ decreases with α. The reason d decreases between α = 1/9 and α = 1/3 while corona density increases is that d does not account for the length of the corona blocks (for α = 1/9, B_1 = 1 while for α = 1/3, B_1 = 3). The one-bead chains do not contribute as much to the density because they are so short and because they are slightly shifted toward the core interior. Otherwise, the behavior shown by d is the same as the maximum corona density, and both are plotted in Figure S3.

The first few beads spend significant time near the peak density, but the last few beads (of a longer corona block) spend more time away from the core and away from the peak density location. The d parameter does not account for this factor and so can only decrease with α. Because this high-density region near the core is the most perturbed, it may be that this region dominates the stretching penalty of the corona block. The first bead moved to create a new block (low α) must necessarily reside in this high-density location. The longer the short block gets as α increases, the easier it is for chains to reside outside this high-density region without additional penalty (see Figure 8c). This means that the first chains that are added may be the most perturbed and carry the greatest penalty. Subsequent added beads reside progressively farther out and so are less perturbed, have a smaller energy penalty for insertion, and therefore affect τ less. This would explain the shape of τ, especially for AB_1B_2 polymers that have no other difference from diblocks; the greatest penalty is paid at low α so the exchange rate (and $\bar{N}_{agg}$ and f_{unimer}) is most greatly affected at low α.

This greater stretching at low α can also be seen in Figure 9, where h_i^2/h_0^2 (h_i is the end-to-end distance) of three-bead segments is plotted as a function of bead index along the corona block ($1 < s_{corona} < N_B$). The ratio h_i^2/h_0^2 is a measure of local stretching, and s_{corona} refers to the center of the three beads used in the h_i calculation; s_{corona} = 1 refers to the bead bonded to the core block, and s_{corona} = N_B refers to the end bead in the block. Because each h_i considers 3 beads, it cannot

DOI: 10.1021/acs.macromol.7b01046
Macromolecules 2017, 50, 6303−6313

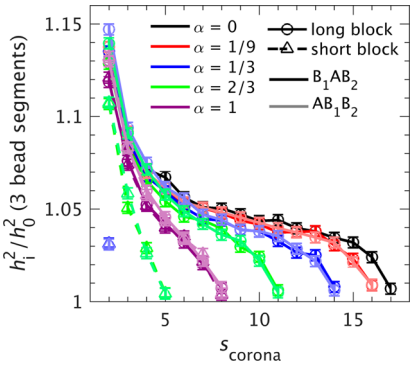

Figure 9. Local stretching (h_i^2/h_0^2 of three bead segments) vs bead position along a corona block (s_{corona}) for B_1AB_2 and AB_1B_2 6−18; χN_{core} = 24.

be calculated for the end beads s_{corona} = 1 and s_{corona} = N_B. The unperturbed end-to-end distance h_0 is measured in a homopolymer melt for N = 3. In each case this local stretching is highest near the core, begins to level off near the middle of the corona block, and then drops near the end of the block. At low s_{corona} a sharp increase occurs very near the core, consistent with the higher density of the corona beads at that location. It is in this region where the greatest chain stretching occurs, and because a higher fraction of beads exist here in the triblock case, the chains are more stretched, resulting in a higher penalty for the inserted state and ultimately faster chain exchange. The middle segments of the corona chains are modestly perturbed with a slightly decreasing perturbation as the beads reach farther away from the core, until the end of the chain is reached, where the chain is nearly unperturbed ($h_i \sim h_0$).

Triblock Exchange in a Diblock-Dominated Environment. A mixture of triblocks and diblocks in solution was simulated in an attempt to separate the chain exchange rate from the environment created by the micellized triblocks and in particular the effects of $\bar{N}_{agg}$ and the denser corona peak. Simulations were run with 5% overall polymer loading as before, but this time 5% of the polymer was triblock and 95% was diblock. One simulation was run mixing AB 6−18 with B_1AB_2 9−6−9, and one simulation was run mixing AB 6−18 with AB_1B_2 6−9−9. Simulations were run with a box size of 82 × 82 × 82 instead of 30 × 30 × 30, resulting in a simulation volume roughly 20 times larger, necessary to get a comparable number of triblock chains in the simulation. 5% triblock polymer resulted in roughly 1 triblock chain per micelle, so that the effect of the triblocks on the overall structure of the micelles was minimal. This results in B_1AB_2 and AB_1B_2 triblocks exchanging in nearly identical environments, so that the effects of core block looping on a single chain pulling out can be separated from the overall effect on $\bar{N}_{agg}$. To measure the exchange rate of only triblocks or diblocks, $F(t)$, the so-called native chain fraction[22] was used instead of $C(t)$. $C(t)$, while conveniently comparable to experimental methods, does not allow measurement of chain exchange of triblocks when there is only one triblock per micelle. At t = 0 all chains in micelles (excluding unimers) were designated as native chains. When a chain is found to have left a micelle, that chain is marked. A chain is detected as having left the micelle when it becomes a unimer or when >50% of the chains in its current micelle are different from the micelle it was in at the previously analyzed step. $F(t)$ is then calculated using

$$F(t) = \left\langle \frac{N_{native}(0) - N_{left}(t)}{N_{native}(0)} \right\rangle \quad (6)$$

where $N_{native}(0)$ refers to the number of chains native to a micelle at t = 0 and $N_{left}(t)$ refers to the number of chains that have left their original micelle at time t. N_{native} and N_{left} include only triblocks when calculated triblock exchange and only diblocks when calculating diblock exchange. This method includes both unimer/dimer extraction and micelle fission/fusion, though fission/fusion was visually observed to be rare.

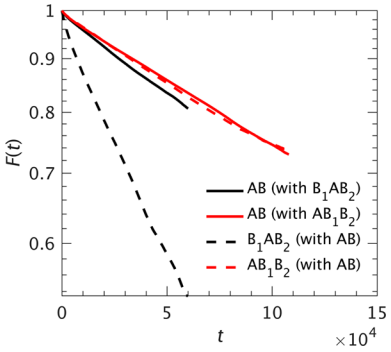

Figure 10. Native chain fraction $F(t)$ for a mixture of AB 6−18 and B_1AB_2 9−6−9 (black) and a mixture of AB 6−18 and AB_1B_2 6−9−9 (red). Mixtures are 5% triblock and 95% diblock, with an overall polymer loading of 5%.

The results for both diblocks and triblocks in both mixed simulations are found in Figure 10. While the B_1AB_2 triblocks exchange much faster than the diblocks (τ_{ABw/B_1AB_2} = 2.87 × 10^5 vs $\tau_{B_1AB_2w/AB}$ = 0.98 × 10^5), the AB_1B_2 triblocks exchange at almost an identical rate as the diblocks (τ_{ABw/B_1AB_2} = 3.48 × 10^5 vs $\tau_{AB_1B_2w/AB}$ = 3.44 × 10^5). Using very asymmetric triblocks (α = 1/9) yields the same results (see Figure S4), except that the difference between B_1AB_2 triblocks and diblocks/AB_1B_2 triblocks is smaller. This is expected based on the results in Figures 2−4, which show the asymmetric triblocks exchanging more slowly than their symmetric analogues. Clearly, the core block topology plays the critical role. The reason the B_1AB_2 triblocks exchange more rapidly here is that the core blocks remain closer to the surface in the case of the B_1AB_2 triblocks, which have a looped core, reducing the enthalpic advantage of the inserted state. This can be seen in Figure 11, where a normalized radial density for each of the polymers in the mixed simulation is plotted. The densities are normalized to the average plateau value in the case of diblocks or the AB_1B_2 polymers and to the peak value in the B_1AB_2 case. This is done for an easier comparison between the triblocks, which only constitute 5% of the overall polymer loading, and the diblocks. It is clear that the B_1AB_2 polymers reside preferentially at the surface of the micelle allowing more rapid expulsion, while both diblocks and AB_1B_2 triblocks extend all the way to the center. This makes sense as the B_1AB_2 core blocks must reach the core in fewer bonds than the unlooped cores. A similar result has been found for tadpole diblock polymers, which also have looped cores and which also exchanged much more rapidly than linear diblocks.[22] Additionally, a looped core block may have lower entropy since two points are effectively pinned to the micelle surface, while only one point is pinned for an

DOI: 10.1021/acs.macromol.7b01046
Macromolecules 2017, 50, 6303−6313

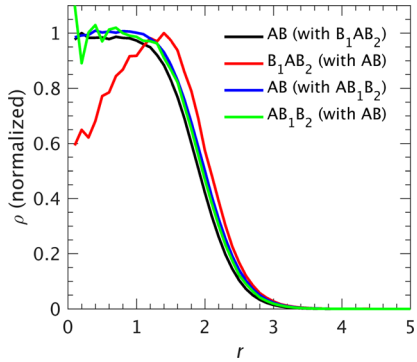

Figure 11. Normalized radial density of A beads (core beads) for mixtures. Diblocks and AB_1B_2 triblocks are normalized to the average of the plateau value, while B_1AB_2 triblocks are normalized to the peak density. In both mixtures, AB 6−18 is used, with B_1AB_2 9−6−9 in one case and AB_1B_2 6−9−9 in the other.

unlooped core block, effectively reducing the number of conformations available for a looped block.[56,57] Both factors would result in smaller $\bar{N}_{agg}$ and f_{unimer} and subsequently faster chain exchange for pure B_1AB_2 micelles vs AB_1B_2 micelles. The corona block differences seem to play a very minor role in the mixed simulations. They limit the maximum micelle size in pure triblock systems, where they increase f_{unimer} and cause more rapid exchange, but within a diblock-dominant environment it has little to no effect on chain exchange. This is reasonable, given the breadth of the N_{agg} distributions seen in Figure 5a; the extra block from a single AB_1B_2 chain affects the corona about as much as a single extra diblock chain, but a shift of 1 in N_{agg} is small given the breadth of the distribution. Still, it is possibly surprising that the localization of this extra corona block and therefore extra density near the AB_1B_2 polymer has such a small effect. Perhaps the density change is simply distributed over the rest of the chains within a micelle, of which there are many more than AB_1B_2 chains.

Pullout Mechanism. The looped nature of the B_1AB_2 triblocks suggests that the pullout mechanism must be rather different than that for the diblocks or AB_1B_2 triblocks. The mechanisms of each were examined by inspection. Simulations of mixed diblocks and triblocks were run, and snapshots were taken at every time step. Because of the very large data requirements of taking so many snapshots, only a few extraction events could be examined, but all looked qualitatively similar. The examples shown here are simply the first extractions observed. Figure 12 shows the progression of the extraction of a diblock copolymer, and Figure 13 shows the progression of the extraction of a B_1AB_2 triblock polymer. The core is shown as a transparent gray surface and is defined using VMD's QuickSurf method, which uses Gaussian densities mapped onto a uniformly spaced lattice to define an isosurface at a particular density, selected such that the isosurface visually matched the surface of the core. Core blocks are shown in red and corona blocks in blue. Movies of each extraction are available in the Supporting Information. In the diblock case (Figure 12), the core blocks pull out bead by bead with a small barrier and a chance of reinsertion at each step. Pauses can often be found as a chain has partly escaped but does not pull all the way out. The AB_1B_2 pullout was similar, as can been seen in the accompanying movie (Supporting Information). The B_1AB_2 triblock, on the other hand, appears to pull out more as a single unit. This is facilitated by the fact that the B_1AB_2 core

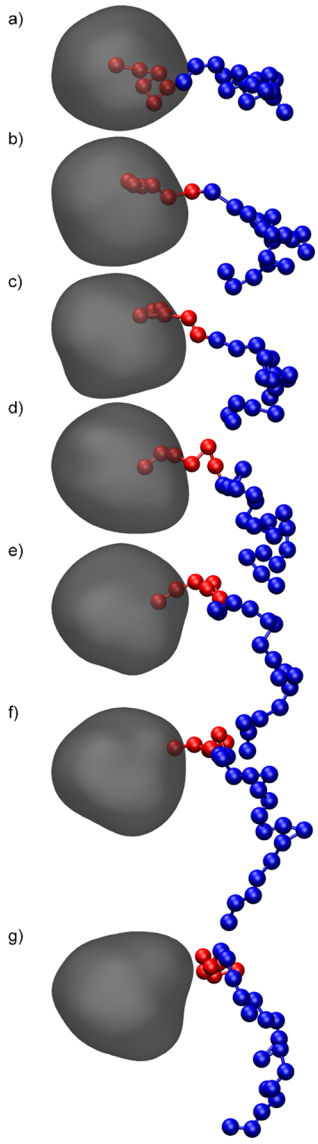

Figure 12. Simulation snapshots of a diblock polymer escaping. The micelle core is shown in gray and determined by a Gaussian distributed average density of A-type beads. A-type beads (core block) are shown in red, and B-type beads (corona block) are shown in blue. (a) shows the core block fully inserted. Each subsequent image shows the pullout of a single bead along the core block until the entire block is removed. The time between pullouts of a single bead varies, with some pulling out rapidly after the preceding bead and others taking a significant amount of time to pull out. AB_1B_2 polymers pull out in a qualitatively similar manner. Accompanying movies for both diblock and AB_1B_2 triblock are available in the Supporting Information. Images are made using VMD[58] and POV-Ray.[59]

block spends significantly more time near the surface of the micelle. The more compact nature of the looped core block may also facilitate extraction, as it decreases the A−B contact area. The unlooped cores do appear to collapse and reduce contact area after extraction, but while escaping at least a portion is still extended. By adopting a typically more compact structure before extraction, the extraction event itself becomes more likely. Coupled with the likely lower entropy of the looped core block as discussed above, these factors result in a significantly increased pullout rate. Tadpole diblocks, which are similar in structure to the B_1AB_2 triblocks in that they both

DOI: 10.1021/acs.macromol.7b01046
Macromolecules 2017, 50, 6303−6313

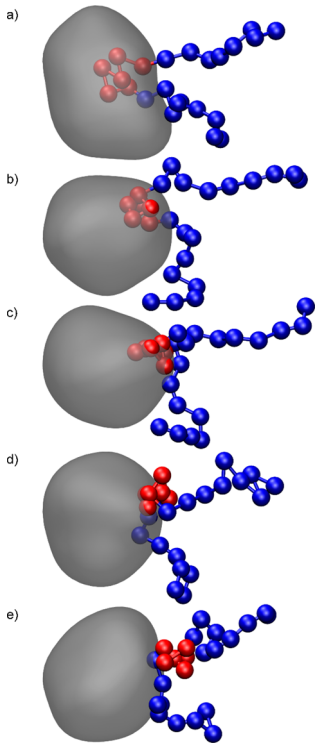

Figure 13. Simulation snapshots of a B_1AB_2 polymer escaping. The micelle core is shown in gray and determined by a Gaussian distributed average density of A-type beads. A-type beads (core block) are shown in red, and B-type beads (corona block) are shown in blue. (a) shows the core block fully inserted. Unlike the diblock and AB_1B_2 chains, the core block beads do not pull out one at a time in sequence. Instead, the entire block appears to come near to the surface of the core and then pull through almost as a single cooperative event. (b) shows the beads near the core surface. (c) shows the beginning of the removal from the core, while (d) and (e) show the completion of the pullout event. An accompanying movie is available in the Supporting Information. Images are made using VMD[58] and POV-Ray.[59]

have a looped core, have also been shown to extract more rapidly than linear diblocks and to reside near the core surface when mixed with diblocks.[23] In that work the tadpole architecture was characterized as effectively reducing χ between the core block and the solvent because of the more compact shape it takes. A more compact shape can be seen in the B_1AB_2 chain extraction case, where a small ball of core beads extracts as one unit rather than one bead at a time (Figure 13 and Supporting Information movie). Thus, this mechanism reduces A−B contact area and effectively reduces χ as found with the tadpole diblocks. It is worth pointing out that although the looped core blocks aid pullout in this case, the fact that very short chains are used limits the possibility of interpenetrating loops, which would hinder pullout. Much longer core blocks (longer than the entanglement length) might exhibit topological hindrances that result in very slow exchange.

In summary, there are two distinct ways by which the looped core (B_1AB_2) triblocks exchange more rapidly than unlooped core triblocks (AB_1B_2) and diblocks: (i) a reduction in $\bar{N}_{agg}$ (see Figure 5b), caused by a reduction in entropy (see discussion of Figure 10), and (ii) localization of the core blocks near the surface and pullout via a single step (as opposed to the multiple activations required for an unlooped core block), resulting in a smaller barrier to pullout. When τ is plotted vs $\bar{N}_{agg}$ in Figure 14, the looped and unlooped core blocks are separated. For the

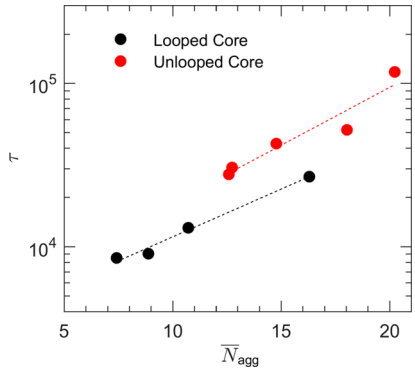

Figure 14. Relaxation time τ vs mean aggregation number $\bar{N}_{agg}$ for looped and unlooped core blocks for chains consisting of 6 A beads and 18 B beads, with χN_{core} = 24. Looped core blocks consist of the B_1AB_2 6−18 series, excluding the diblock, and the unlooped core blocks consist of the AB_1B_2 6−18 series. Dashed lines are exponential fits found using least-squares.

same overall chain size, composition, and χ, looped core blocks consistently exchange more rapidly, even at identical $\bar{N}_{agg}$. This is explained by the pullout mechanism described above and in Figures 12 and 13.

CONCLUSIONS

Dissipative particle dynamics simulations were used to study the kinetics of chain exchange in micelles formed by asymmetric and symmetric B_1AB_2 and AB_1B_2 triblock copolymers. It was found that both types of triblocks exchanged much more rapidly than corresponding diblocks of equivalent core block length and overall length, but B_1AB_2 triblocks exchange much faster than AB_1B_2 triblocks. Though the chain exchange rate dropped rapidly from diblock to triblock, the rate only decreased modestly as a function of asymmetry α, with very asymmetric triblocks ($\alpha \approx 0$) exchanging slightly slower than symmetric triblocks ($\alpha = 1$). The exchange rates correlate strongly with the average aggregation number $\bar{N}_{agg}$ and with the unimer fraction f_{unimer}, indicating that chain exchange is primarily determined by the free energy difference between inserted and free states.

There are two main causes for this change in free energy and exchange rate for B_1AB_2 copolymers: (1) a higher density/stretching of corona blocks near the core surface and (2) looping of the core blocks, which leads to easier extraction and a smaller free energy benefit to insertion. The triblock architecture increases the number of corona blocks per micelle for a given $\bar{N}_{agg}$, which means that the density of corona chains is increased, especially near the micelle core. Because this increased stretching is concentrated near the micelle core, it is greatest for corona beads that have only a few bonds (~3 or 4 for the conditions used here) separating them from the core block. As long as α is large enough (~1/3 in this case) the extra beads do little to affect stretching. At lower α values these beads are still being added, and so the largest change in exchange rate occurs at low α.

The looped core blocks in B_1AB_2 polymers reduce the entropy of the inserted state and shrink $\bar{N}_{agg}$, resulting in more rapid chain exchange. This effect is also somewhat independent of asymmetry since looping occurs regardless of differences in corona block lengths. While AB_1B_2 polymers are affected by the higher density/stretching of the corona blocks near the core, they are not affected by a looped core block, and so exchange

DOI: 10.1021/acs.macromol.7b01046
Macromolecules 2017, 50, 6303−6313

more slowly and have larger $\bar{N}_{agg}$. In a diblock-dominated environment, where the overall corona block density and $\bar{N}_{agg}$ are independent of the triblock architecture, the changes caused by the looped configuration dominate triblock chain exchange differences: AB_1B_2 polymers exchange at the same rate as diblocks, while B_1AB_2 polymers exchange much faster. This core block looping also results in a different extraction mechanism, whereby the chains do not pull out in a series of activation steps, but more as a single compact globule, facilitating chain exchange and resulting in looped core blocks exchanging more rapidly than unlooped core blocks even for identical $\bar{N}_{agg}$. These results provide insight into the thermodynamics and kinetics of micelle chain exchange in triblock polymers and can guide further development of useful triblock micelle systems.

■ ASSOCIATED CONTENT

Supporting Information

The Supporting Information is available free of charge on the ACS Publications website at DOI: 10.1021/acs.macromol.7b01046.

Further examples of distribution of aggregation numbers, corona chain densities, and relaxation functions (PDF)

Movie showing extraction of a diblock copolymer (MPG)

Movie showing extraction of a B_1AB_2 triblock polymer (MPG)

Movie showing extraction of a AB_1B_2 triblock polymer (MPG)

■ AUTHOR INFORMATION

Corresponding Author

*E-mail lodge@umn.edu.

ORCID

Andrew J. Peters: 0000-0001-5031-2828

Timothy P. Lodge: 0000-0001-5916-8834

Notes

The authors declare no competing financial interest.

■ ACKNOWLEDGMENTS

This work was supported by the National Science Foundation, Polymers Program (DMR-1206459 and 1707578). All simulations were conducted using the resources of the Minnesota Supercomputing Institute (MSI) at the University of Minnesota.

■ REFERENCES

(1) Riess, G. Micellization of Block Copolymers. *Prog. Polym. Sci.* **2003**, *28*, 1107−1170.

(2) Halperin, A.; Tirrell, M.; Lodge, T. P. Tethered Chains in Polymer Microstructures. In *Macromolecules: Synthesis, Order and Advanced Properties*; Springer: 1992.

(3) Gohy, J.-F. Block Copolymer Micelles. In *Block Copolymers II*; Abetz, V., Ed.; Springer: Berlin, 2005.

(4) Zana, R. *Dynamics of Surfactant Self-Assemblies: Micelles, Microemulsions, Vesicles, and Lyotropic Phases*; CRC Press: 2005.

(5) Schouten, M.; Dorrepaal, J.; Stassen, W. J. M.; Vlak, W. A. H. M.; Mortensen, K. Thermal Stability of Polystyrene-*b*-Poly(ethylene/propylene) Diblock Copolymer Micelles in Paraffinic Solvents. *Polymer* **1989**, *30*, 2038−2046.

(6) Anderson, W. Block Copolymers as Viscosity Index Improvers for Lubricating Oils. US3763044A, 1973.

(7) Baines, F. L.; Dionisio, S.; Billingham, N. C.; Armes, S. P. Use of Block Copolymer Stabilizers for the Dispersion Polymerization of Styrene in Alcoholic Media. *Macromolecules* **1996**, *29*, 3096−3102.

(8) Honda, C.; Hasegawa, Y.; Hirunuma, R.; Nose, T. Micellization Kinetics of Block Copolymers in Selective Solvent. *Macromolecules* **1994**, *27*, 7660−7668.

(9) Willner, L.; Poppe, A.; Allgaier, J.; Monkenbusch, M.; Richter, D. Time-resolved SANS for the determination of unimer exchange kinetics in block copolymer micelles. *Europhys. Lett.* **2001**, *55*, 667.

(10) Choi, S. H.; Lodge, T. P.; Bates, F. S. Mechanism of Molecular Exchange in Diblock Copolymer Micelles: Hypersensitivity to Core Chain Length. *Phys. Rev. Lett.* **2010**, *104*, 1−4.

(11) Lu, J.; Bates, F. S.; Lodge, T. P. Remarkable Effect of Molecular Architecture on Chain Exchange in Triblock Copolymer Micelles. *Macromolecules* **2015**, *48*, 2667−2676.

(12) Zinn, T.; Willner, L.; Lund, R.; Pipich, V.; Richter, D. Equilibrium Exchange Kinetics in n-alkyl−PEO Polymeric Micelles: Single Exponential Relaxation and Chain Length Dependence. *Soft Matter* **2012**, *8*, 623.

(13) Lund, R.; Willner, L.; Richter, D. Kinetics of Block Copolymer Micelles Studied by Small-Angle Scattering Methods. In *Controlled Polymerization and Polymeric Structures: Flow Microreactor Polymerization, Micelles Kinetics, Polypeptide Ordering, Light Emitting Nanostructures*; Abe, A., Lee, K.-S., Leibler, L., Kobayashi, S., Eds.; Springer International Publishing: Cham, 2013; pp 51−158.

(14) Lund, R.; Willner, L.; Monkenbusch, M.; Panine, P.; Narayanan, T.; Colmenero, J.; Richter, D. Structural Observation and Kinetic Pathway in the Formation of Polymeric Micelles. *Phys. Rev. Lett.* **2009**, *102*, 188301.

(15) Zhu, Z.; Armes, S. P.; Liu, S. pH-Induced Micellization Kinetics of ABC Triblock Copolymers Measured by Stopped-Flow Light Scattering. *Macromolecules* **2005**, *38*, 9803−9812.

(16) Zhang, J.; Xu, J.; Liu, S. Chain-Length Dependence of Diblock Copolymer Micellization Kinetics Studied by Stopped-Flow pH-Jump. *J. Phys. Chem. B* **2008**, *112*, 11284−11291.

(17) Rao, J.; Zhang, J.; Xu, J.; Liu, S. Cononsolvency-Induced Micellization Kinetics of Pyrene End-Labeled Diblock Copolymer of *N*-Isopropylacrylamide and Oligo(ethylene Glycol) Methyl Ether Methacrylate Studied by Stopped-Flow Light-Scattering and Fluorescence. *J. Colloid Interface Sci.* **2008**, *328*, 196−202.

(18) Wang, Y.; Kausch, C. M.; Chun, M.; Quirk, R. P.; Mattice, W. L. Exchange of Chains between Micelles of Labeled Polystyrene-*block*-poly(oxyethylene) As Monitored by Nonradiative Singlet Energy Transfer. *Macromolecules* **1995**, *28*, 904−911.

(19) Peters, A. J.; Lodge, T. P. Comparison of Gel Relaxation Times and End-Block Pullout Times in ABA Triblock Copolymer Networks. *Macromolecules* **2016**, *49*, 7340−7349.

(20) Zinn, T.; Willner, L.; Lund, R. Telechelic Polymer Hydrogels: Relation between the Microscopic Dynamics and Macroscopic Viscoelastic Response. *ACS Macro Lett.* **2016**, *5*, 1353−1356.

(21) Li, Z.; Dormidontova, E. E. Kinetics of Diblock Copolymer Micellization by Dissipative Particle Dynamics. *Macromolecules* **2010**, *43*, 3521−3531.

(22) Li, Z.; Dormidontova, E. E. Equilibrium Chain Exchange Kinetics in Block Copolymer Micelle Solutions by Dissipative Particle Dynamics Simulations. *Soft Matter* **2011**, *7*, 4179.

(23) Prhashanna, A.; Dormidontova, E. E. Tadpole and Mixed Linear/Tadpole Micelles of Diblock Copolymers: Thermodynamics and Chain Exchange Kinetics. *Macromolecules* **2017**, *50*, 1740−1748.

(24) Prhashanna, A.; Khan, S. A.; Chen, S. B. Kinetics of Chain Exchange between Diblock Copolymer Micelles. *Macromol. Theory Simul.* **2016**, *25*, 383−391.

(25) Prhashanna, A.; Chen, S. B. Chain Exchange Kinetics between Linear ABA-Type Triblock Copolymer Micelles. *Polymer* **2017**, *118*, 22−29.

(26) Haliloğlu, T.; Bahar, I.; Erman, B.; Mattice, W. L. Mechanisms of the Exchange of Diblock Copolymers between Micelles at Dynamic Equilibrium. *Macromolecules* **1996**, *29*, 4764−4771.

DOI: 10.1021/acs.macromol.7b01046
Macromolecules 2017, 50, 6303−6313

(27) Chang, K.; Macosko, C. W.; Morse, D. C. Interfacial Tension Measurement and Micellization in a Polymer Blend with Copolymer Surfactant: A False Critical Micelle Concentration. *Macromolecules* **2015**, *48*, 8154−8168.
(28) Lu, J.; Choi, S.; Bates, F. S.; Lodge, T. P. Molecular Exchange in Diblock Copolymer Micelles: Bimodal Distribution in Core-Block Molecular Weights. *ACS Macro Lett.* **2012**, *1*, 982−985.
(29) Underhill, R. S.; Ding, J.; Birss, V. I.; Liu, G. Chain Exchange Kinetics of Polystyrene-*block*-poly(2-cinnamoylethyl methacrylate) Micelles in THF/Cyclopentane Mixtures. *Macromolecules* **1997**, *30*, 8298−8303.
(30) Zinn, T.; Willner, L.; Pipich, V.; Richter, D.; Lund, R. Molecular Exchange Kinetics of Micelles: Corona Chain Length Dependence. *ACS Macro Lett.* **2016**, *5*, 884−888.
(31) Ma, Y.; Lodge, T. P. Chain Exchange Kinetics in Diblock Copolymer Micelles in Ionic Liquids: The Role of χ. *Macromolecules* **2016**, *49*, 9542−9552.
(32) Tian, M.; Qin, A.; Ramireddy, C.; Webber, S. E.; Munk, P.; Tuzar, Z.; Prochazka, K. Hybridization of Block Copolymer Micelles. *Langmuir* **1993**, *9*, 1741−1748.
(33) Lund, R.; Willner, L.; Richter, D.; Dormidontova, E. E. Equilibrium Chain Exchange Kinetics of Diblock Copolymer Micelles: Tuning and Logarithmic Relaxation. *Macromolecules* **2006**, *39*, 4566−4575.
(34) Kang, M.; Lam, D.; Discher, D. E.; Loverde, S. M. Molecular Modeling of Block Copolymer Self-Assembly and Micellar Drug Delivery. In *Computational Pharmaceutics*; John Wiley & Sons, Ltd.: 2015; pp 53−80.
(35) de Graaf, A. J.; Boere, K. W. M.; Kemmink, J.; Fokkink, R. G.; van Nostrum, C. F.; Rijkers, D. T. S.; van der Gucht, J.; Wienk, H.; Baldus, M.; Mastrobattista, E.; et al. Looped Structure of Flowerlike Micelles Revealed by 1H NMR Relaxometry and Light Scattering. *Langmuir* **2011**, *27*, 9843−9848.
(36) Hoogerbrugge, P. J.; Koelman, J. M. V. A. Simulating Microscopic Hydrodynamic Phenomena with Dissipative Particle Dynamics. *EPL* **1992**, *19*, 155.
(37) Groot, R. D.; Warren, P. B. Dissipative Particle Dynamics: Bridging the Gap between Atomistic and Mesoscopic Simulation. *J. Chem. Phys.* **1997**, *107*, 4423−4435.
(38) Spaeth, J. R.; Kevrekidis, I. G.; Panagiotopoulos, A. Z. Dissipative Particle Dynamics Simulations of Polymer-Protected Nanoparticle Self-Assembly. *J. Chem. Phys.* **2011**, *135*, 184903.
(39) Spaeth, J. R.; Kevrekidis, I. G.; Panagiotopoulos, A. Z. A Comparison of Implicit- and Explicit-Solvent Simulations of Self-Assembly in Block Copolymer and Solute Systems. *J. Chem. Phys.* **2011**, *134*, 164902.
(40) Khani, S.; Jamali, S.; Boromand, A.; Hore, M. J. A.; Maia, J. Polymer-Mediated Nanorod Self-Assembly Predicted by Dissipative Particle Dynamics Simulations. *Soft Matter* **2015**, *11*, 6881−6892.
(41) Posel, Z.; Limpouchová, Z.; Šindelka, K.; Lísal, M.; Procházka, K. Dissipative Particle Dynamics Study of the pH-Dependent Behavior of Poly(2-Vinylpyridine)-Block-Poly(ethylene Oxide) Diblock Copolymer in Aqueous Buffers. *Macromolecules* **2014**, *47*, 2503−2514.
(42) Kang, M.; Lam, D.; Discher, D. E.; Loverde, S. M. Molecular Modeling of Block Copolymer Self-Assembly and Micellar Drug Delivery. In *Computational Pharmaceutics*; John Wiley & Sons, Ltd.: 2015; pp 53−80.
(43) Español, P.; Warren, P. Statistical Mechanics of Dissipative Particle Dynamics. *EPL* **1995**, *30*, 191.
(44) Anderson, J. A.; Lorenz, C. D.; Travesset, A. General Purpose Molecular Dynamics Simulations Fully Implemented on Graphics Processing Units. *J. Comput. Phys.* **2008**, *227*, 5342−5359.
(45) Glaser, J.; Nguyen, T. D.; Anderson, J. A.; Lui, P.; Spiga, F.; Millan, J. A.; Morse, D. C.; Glotzer, S. C. Strong Scaling of General-Purpose Molecular Dynamics Simulations on GPUs. *Comput. Phys. Commun.* **2015**, *192*, 97−107.
(46) Phillips, C. L.; Anderson, J. A.; Glotzer, S. C. Pseudo-Random Number Generation for Brownian Dynamics and Dissipative Particle Dynamics Simulations on GPU Devices. *J. Comput. Phys.* **2011**, *230*, 7191−7201.
(47) Marrink, S. J.; Tieleman, D. P.; Mark, A. E. Molecular Dynamics Simulation of the Kinetics of Spontaneous Micelle Formation. *J. Phys. Chem. B* **2000**, *104*, 12165−12173.
(48) Wang, E.; Lu, J.; Bates, F. S.; Lodge, T. P. Effect of Corona Block Length on Micelle Chain Exchange Kinetics. Unpublished.
(49) Halperin, A.; Alexander, S. *Macromolecules* **1989**, *22*, 2403−2412.
(50) Lu, J.; Bates, F. S.; Lodge, T. P. Addition of Corona Block Homopolymer Retards Chain Exchange in Solutions of Block Copolymer Micelles. *Macromolecules* **2016**, *49*, 1405−1413.
(51) Zinn, T.; Willner, L.; Pipich, V.; Richter, D.; Lund, R. Molecular Exchange Kinetics of Micelles: Corona Chain Length Dependence. *ACS Macro Lett.* **2016**, *5*, 884−888.
(52) Milner, S. T. Polymer Brushes. *Science* **1991**, *251*, 905−914.
(53) Moh, L. C. H.; Losego, M. D.; Braun, P. V. Solvent Quality Effects on Scaling Behavior of Poly(methyl Methacrylate) Brushes in the Moderate- and High-Density Regimes. *Langmuir* **2011**, *27*, 3698−3702.
(54) Smith, G. D.; Bedrov, D. Dispersing Nanoparticles in a Polymer Matrix: Are Long, Dense Polymer Tethers Really Necessary? *Langmuir* **2009**, *25*, 11239−11243.
(55) Kumar, S. K.; Jouault, N.; Benicewicz, B.; Neely, T. Nanocomposites with Polymer Grafted Nanoparticles. *Macromolecules* **2013**, *46*, 3199−3214.
(56) Balsara, N. P.; Tirrell, M.; Lodge, T. P. Micelle Formation of BAB Triblock Copolymers in Solvents That Preferentially Dissolve the A Block. *Macromolecules* **1991**, *24*, 1975−1986.
(57) De Jeu, W.; Lambooy, P.; Hamley, I. W.; Vaknin, D.; Pedersen, J. S.; Kjaer, K.; Seyger, R.; Van Hutten, P.; Hadziioannou, G. On the Morphology of a Lamellar Triblock Copolymer Film. *J. Phys. II* **1993**, *3*, 139.
(58) Humphrey, W.; Dalke, A.; Schulten, K. VMD: Visual Molecular Dynamics. *J. Mol. Graphics* **1996**, *14*, 33−38.
(59) Persistence of Vision Pty. Ltd., Persistence of Vision Raytracer 2004, Version 3.6. Retrieved from http://www.povray.org/download/.

DOI: 10.1021/acs.macromol.7b01046
Macromolecules 2017, 50, 6303−6313